Supporting Information

Tracking Polarization and Passivation in Anion Exchange Membrane Electrolyzers via Current-Dependent Distribution of Relaxation Times of Electrochemical Impedance Spectroscopy

Elisabetta Campedelli[a], Enrico Squizzato[b], Marzio Rancan[c], Christian Durante*[,a]

[a] Department of Chemical Sciences, University of Padova, via Marzolo 1, 35131, Padova, Italy.
[b] Pietro Fiorentini S.p.A., Via Enrico Fermi 8/10, 36057, Arcugnano (VI), Italy.
[c] Institute of Condensed Matter Chemistry and Technologies for Energy (ICMATE), National Council (CNR) c/o Department of Chemical Sciences, University of Padova, Via Marzolo 1, 35131, Padova, Italy.
* E-mail: christian.durante@unipd.it.

S1. Kramers-Kronig analysis

The Kramers–Kronig consistency tests were performed using the Linear Kramers-Kronig (Lin-KK) validity test software available from the Karlsruhe Institute of Technology (KIT) and based on the method proposed by Schonleber et al. [1]

Before the DRT analysis, the Kramers–Kronig (K–K) relationship was used to verify the reliability of all EIS data acquired in our study. The K-K residuals at each frequency for the EIS data acquired at 0.1 A are reported in Figure S1a-c for the EIS spectra acquired before the stability test and after 24h and 48h of operation. The residuals of both real and imaginary components are within the ± 1%, confirming that the system follows the principles of causality, linearity, and stability. The residuals of all the other measurements remain within the ± 1% interval, confirming overall compliance with the principles of casuality, linearity and stability. The discussion will focus on the K-K residuals of the 1.2 A measurement, as this was the only case showing anomalous non-linear EIS behavior. The K-K residuals for the EIS data at 1.2 A are shown in Figure S1d-f at each step of the stability test (before, after 24 h and after 48 h of operation). For the EIS spectra at 1.2 A before the test (Figure 2d), the real and imaginary residuals are below ± 1%, indicating good agreement with the expected physical behavior. However, after 24 h and 48 h the residuals increased to within ± 4%, indicating a reasonable agreement between the model and the experimental data, although with slightly reduced accuracy compared to ideal conditions. This behavior was expected for the low-frequency range since the corresponding Nyquist plots (see Figure 4f of the manuscript) show scattered EIS data. On the other hand, above 0.07 Hz, the residuals of both real and imaginary components remain within ± 1%.

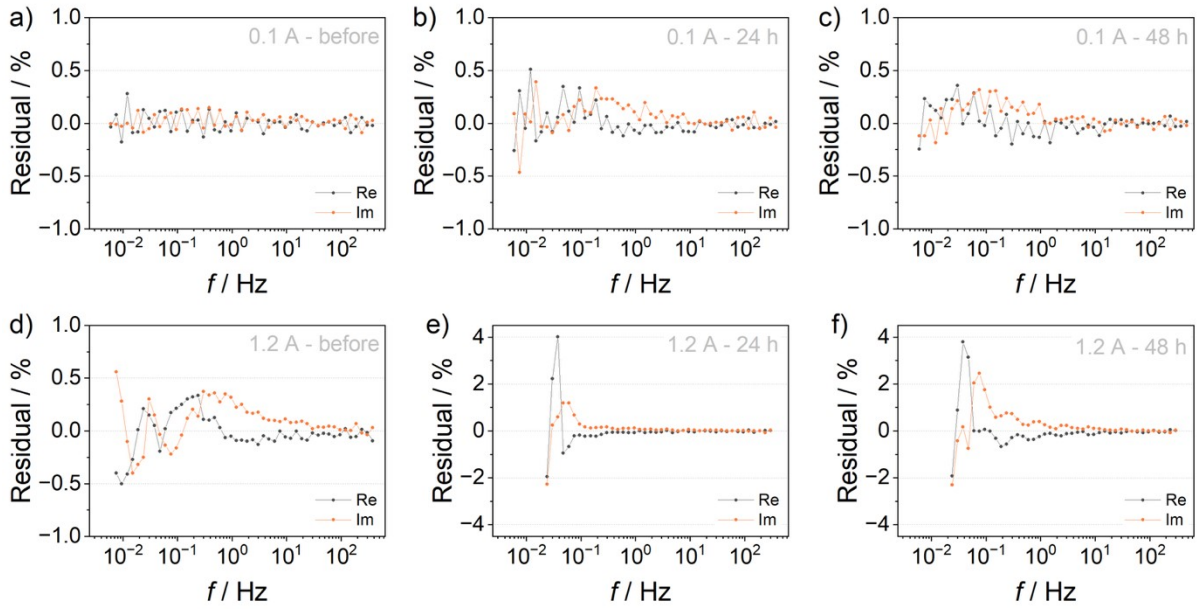

Figure S1 – a-c) Kramers–Kronig analysis residuals of the impedance data. Residuals of the real and imaginary components at 0.1 A before the stability test, after 24 h, and after 48 h of the stability test. d-e) Kramers–Kronig analysis residuals of the impedance data. Residuals of the real and imaginary components at 1.2 A before the stability test, after 24 h, and after 48 h of the stability test.

S2. Analysis of the regularization parameter λ

In general, higher values of λ lead to a smoother DRT response but may hide relevant impedance features, whereas lower values of λ tend to overfit the data and introduce artificial oscillations (and artefactual as highlighted by you).

For the case of 0.1 A (Figure S2a), the low-frequency peak (assigned to the anode) increases in intensity as λ decreases, while the high-frequency peak (associated with ion transport) remains almost unchanged. The mid-frequency peak is not visible at $\lambda = 10^{-1}$, however becomes clearly defined from $\lambda=10^{-2}$ onwards. The residual analysis (Figures S2c-d) shows that for $\lambda \leq 10^{-3}$ the real and imaginary residuals remain low and without significant differences, indicating a stable and reliable fit.

At higher current (0.5 A, Figure S2e), the mid-frequency peak is clearly observed only for $\lambda=10^{-3}$ and 10^{-4}. However, the residuals (Figures S2g-h) do not show significant differences between the tested values of λ, confirming the robustness of the fitting.

Based on this analysis, the regularization parameter was set to $\lambda=10^{-3}$, as it provides a good compromise between fitting accuracy and smoothing of the DRT response, without introducing artefacts in the reconstructed DRT.

In addition, DRT analysis of the EIS spectra at 0.1 A after 48 h of testing is shown in Figure S3 using different regularization parameters. The same observations reported for Figure S2 are also valid here.

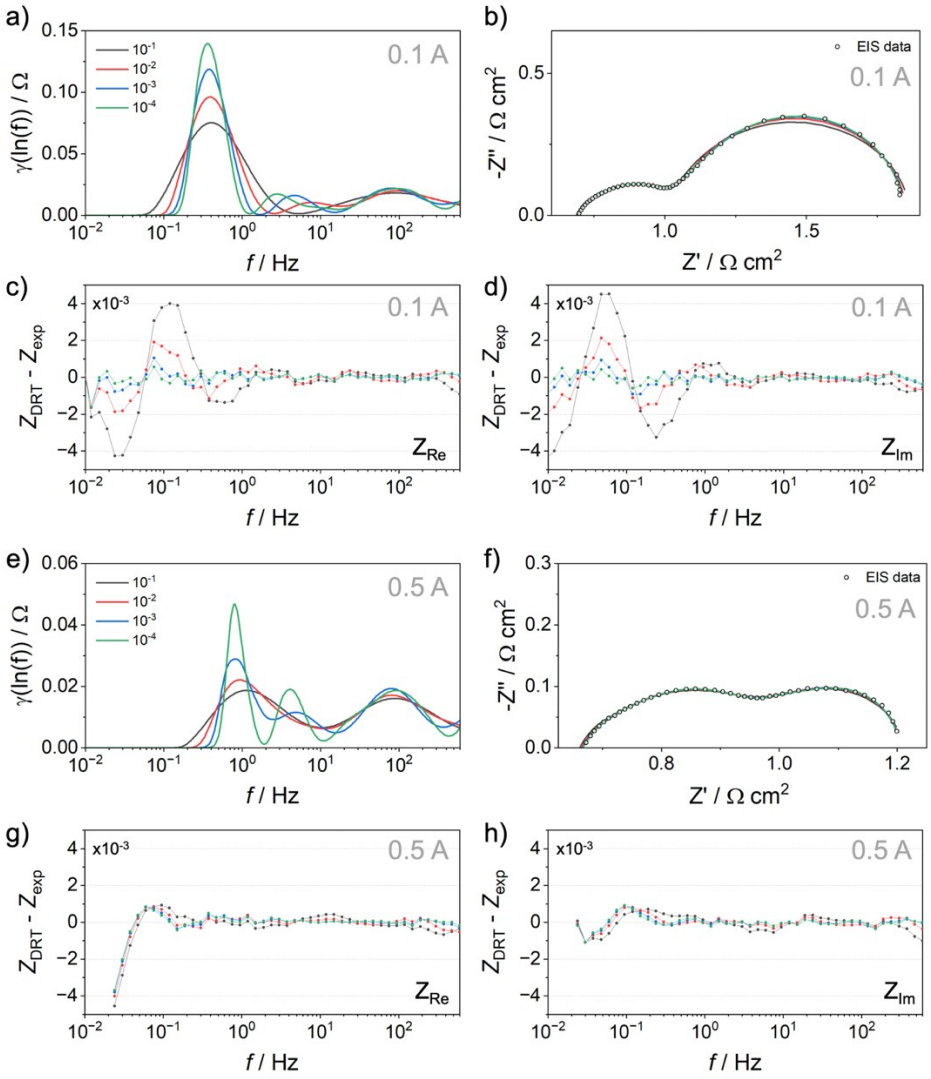

Figure S2 – a-b) DRT curves of 0.1 A (before the test) calculated using different regularization parameters (from 10^{-1} to 10^{-4}) and the corresponding EIS reconstructed from the DRT fitting. The corresponding residuals of the real and imaginary components are shown in c) and d), respectively. e-f) DRT curves of 0.5 A (before the test) obtained using different regularization parameters the corresponding EIS reconstructed. The corresponding residuals of the real and imaginary components are shown in g) and h), respectively.

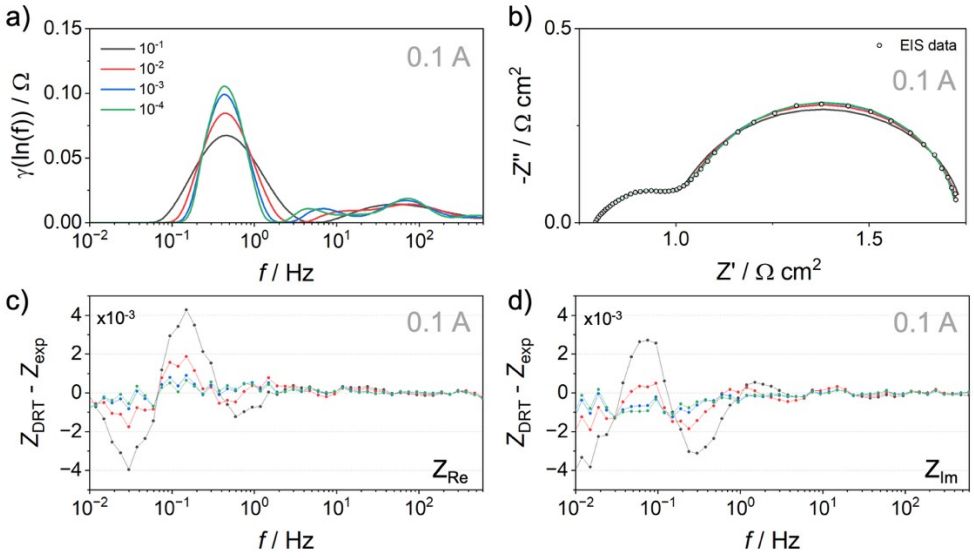

Figure S3 – a-b) DRT curves of 0.1 A (after 48 h) calculated using different regularization parameters (from 10^{-1} to 10^{-4}) and the corresponding EIS reconstructed from the DRT fitting. The corresponding residuals of the real and imaginary components are shown in c) and d), respectively.

S3. DRT deconvolution and fitting criteria

The DRT curves were deconvoluted by nonlinear least-squares fitting using multiple Gaussian functions in the Multiple Peak Fit module of OriginPro (OriginLab, version 10.3). The baseline was fixed to zero, the peaks were selected manually, and the goodness of fit was evaluated from the R^2 values.

The area under each peak was calculated by integrating γ(lnf) versus lnf as shown in Equation S1, yielding the resistance $R_{p,i}$ associated with the corresponding i-th polarization process:

$$R_{p,\,i} = \int_{f_{1,i}}^{f_{2,i}} \gamma(\ln f)\, d(\ln f) \qquad \text{Equation (S1)}$$

where $f_{1,i}$ and $f_{2,i}$ are the lower and upper limits of the relaxation times associated with the i-th DRT peak. The sum of all $R_{p,i}$ values correspond to the total polarization resistance R_p.

To better valuate the different approaches for handling the inductance contribution in DRT analysis, the effect of each choice on the quantification of the high frequency peak is provided here. The DRT curves obtained using the three fitting approaches presented in Figure 3a-d together with the corresponding deconvoluted ion transport peaks are reported in Figure S3 for each fitting method. The characteristic frequency and resistance values are reported in Table S1 together with the corresponding fitting errors. For all approaches, the multiple Gaussian fitting accurately reproduces the DRT response, as confirmed by the high coefficients of determination reported in Table S1 ($R^2 > 0.99$ in all cases), demonstrating the reliability of the deconvolution approach.

From these results, the truncation was found to affect only partially the ion transport resistance values, with a difference of approximately 0.005 Ω. Since this value was not used as an absolute

quantity but only to evaluate the relative decrease in ion transport resistance associated with the break-in effect and considering that the difference was derived from two DRT curves truncated using the same procedure, the obtained results and deconvolution can be considered reliable.

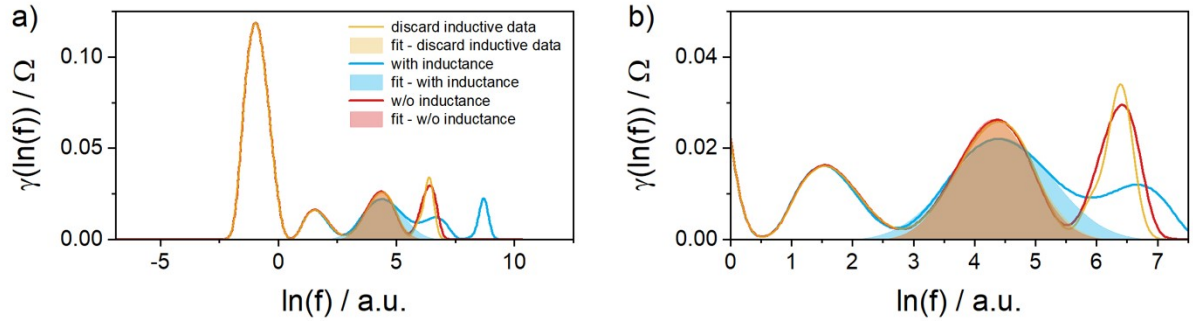

Figure S4 – a) DRT curves at 0.1 A obtained using the three fitting approaches presented in the manuscript. Peak deconvolution was applied to each DRT curve, and the deconvoluted ion transport peaks are reported for each fitting approach. b) Enlarged view of the frequency region corresponding to the ion transport peak.

Table S1 – Characteristic frequency and resistance of the ion transport process identified from the EIS measurement acquired at 0.1 A. The values were obtained from the peak deconvolution of the DRT curves shown in Figure 1, and the corresponding fitting errors are also reported.

	f_c / Hz	**R / Ω**	**R^2 / a.u.**
discard inductive data	77 ± 1	0.0412 ± 0.0007	0.994
with inductance	85 ± 1	0.0475 ± 0.0009	0.995
w/o inductance	75 ± 1	0.0408 ± 0.0006	0.995

S4. Additional investigation of the ion transport peak

To further confirm the nature of the high-frequency peak, which was assigned to ion transport in the manuscript, an additional experiment by replacing the cathodic catalyst layer composed of Pt/C+PTFE with a modified cathode containing both PTFE and ionomer was performed. The Pt loading was kept constant at 0.5 mg cm^{-2}, as confirmed by the supplier. The comparison is reported in Figure S5: "PTFE" refers to the test performed with Pt/C containing only PTFE, while "PTFE + Ionomer" refers to the test where both PTFE and ionomer were included in the catalyst layer.

Figure S5b shows that the OER and HER peaks are very similar to those already reported in the manuscript. Their trends as a function of current are also consistent with the previous results. However, the ion transport peak no longer remains constant: it shifts toward higher

frequencies with increasing current, while its resistance decreases. This behaviour differs from that observed in the manuscript, where the ion transport contribution remained almost constant (Figure S5a).

Figure S5c compares the PTFE and PTFE+Ionomer tests at 0.1 A (the corresponding iR-corrected cell potential is also reported). In general, the same peak distribution can be observed, which is reasonable since the cell setup and catalysts are identical. However, the ion transport peak is significantly larger in the PTFE+Ionomer configuration, consistent with the fact that ion transport is directly affected by the presence of ionomer in the catalyst layer.

Furthermore, Figures S5d-e report the frequency and resistance trends of the ion transport peak as a function of current for both the PTFE and PTFE+Ionomer tests. These results clearly show that the PTFE+ionomer cell exhibits a stronger current dependence: the characteristic frequency increases with increasing current density because higher current requires the transport of a larger amount of OH^- ions, leading to a greater activation of the anion-conducting pathways and consequently leaving more active sites available for the HER reaction. Accordingly, the ion transport resistance decreases with increasing current, and this effect is more pronounced in the PTFE+ionomer cell. However, a comparison between the two configurations indicates that the PTFE cell exhibits a lower ion transport resistance. This trend is also consistent with the iR-corrected polarization curves reported in Figure S5e. Overall, these results suggest that, in this specific electrode configuration, the addition of ionomer modifies the catalyst layer structure, which may partially hinder access to HER active sites while simultaneously affecting the ion transport pathways.

Each test was repeated twice, and the results confirm good reproducibility, as well as the additional voltage required when the ionomer is added to the Pt/C catalyst layer.

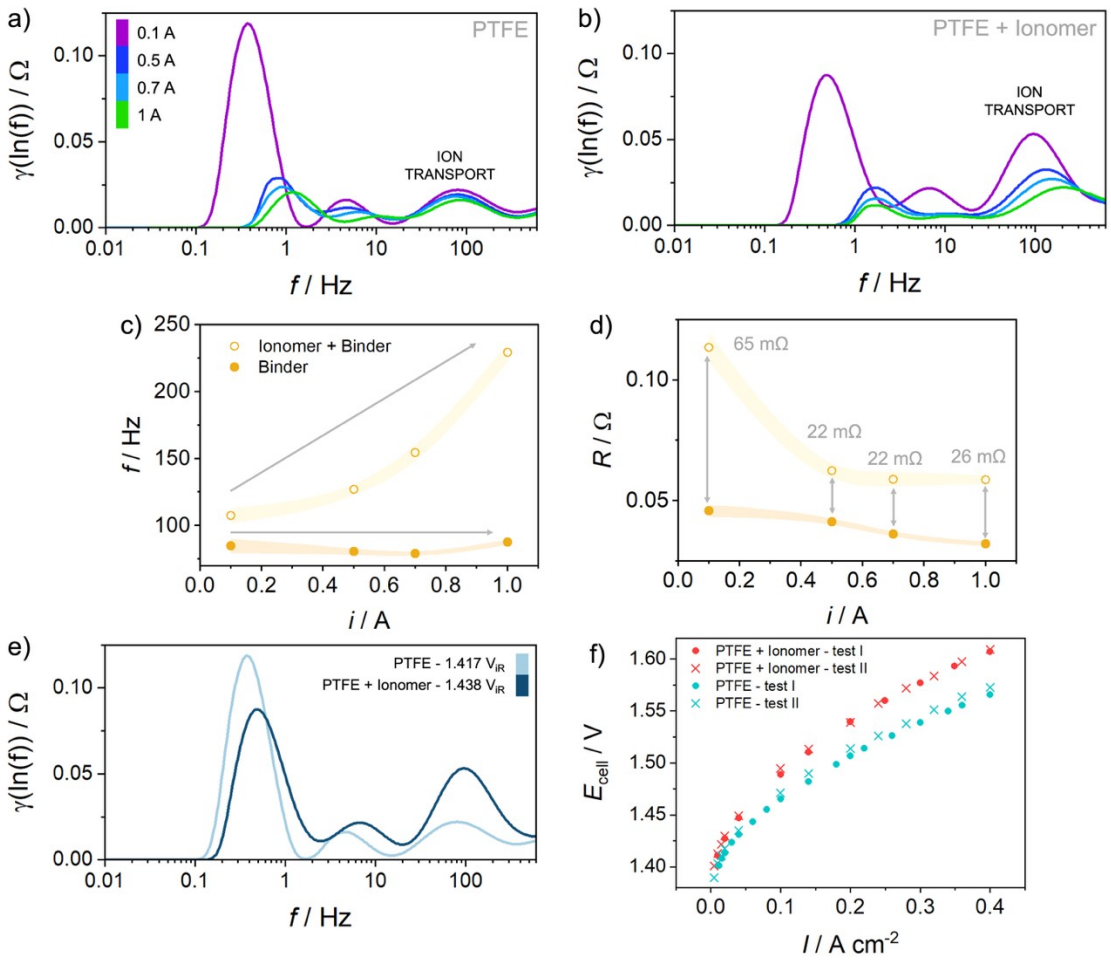

Figure S5 – a-b) DRT curves at different applied currents for the test performed with Pt/C containing only PTFE and containing PTFE+Ionomer, respectively. c-d) The characteristic frequency and resistance values of the ion transport process in function of the applied currents, respectively. e) Comparison of the test performed with Pt/C containing only PTFE (light blue) and containing PTFE+Ionomer (blue) at the applied current of 0.1 A. The iR-corrected cell potential values are reported, as well. f) Polarization curves of the PTFE and PTFE+Ionomer configurations repeated twice. The cell potential values are iR-corrected.

Supporting Information References

1 M. Schönleber, D. Klotz and E. Ivers-Tiffée, *Electrochimica Acta*, 2014, **131**, 20–27.